Divacancy in 4H-SiC

N. T. Son, P. Carlsson, J. ul Hassan, and E. Janzén
Department of Physic, Chemistry and Biology, Linköping University, SE-581 83 Linköping, Sweden

T. Umeda and J. Isoya
Graduate School of Library, Information and Media Studies, University of Tsukuba, Tsukuba 305-8550, Japan

A. Gali
Department of Atomic Physics, Budapest University of Technology and Economics, H-1111 Budapest, Hungary

M. Bockstedte
Universität Erlangen-Nürnberg, D-91058, Erlangen, Germany, and Universidad del País Vasco, E-20018, San Sebastián, Spain

N. Morishita, T. Ohshima, and H. Itoh
Japan Atomic Energy Research Institute, Takasaki 370-1292, Japan

(Received 22 July 2005; revised manuscript received 12 December 2005; published 6 February 2006; corrected 7 February 2006)

Electron paramagnetic resonance and *ab initio* supercell calculations suggest that the $P6/P7$ centers, which were previously assigned to the photoexcited triplet states of the carbon vacancy-antisite pairs in the double positive charge state, are related to the triplet ground states of the neutral divacancy. The spin density is found to be located mainly on three nearest C neighbors of the silicon vacancy, whereas it is negligible on the nearest Si neighbors of the carbon vacancy.

DOI: 10.1103/PhysRevLett.96.055501 PACS numbers: 61.72.Ji, 61.72.Bb, 71.15.Mb, 76.30.Mi

Divacancies are common defects in semiconductors comprised of neighboring isolated vacancies. For SiC, an unambiguous identification of this defect that has been predicted to be thermally stable [1–3] is so far missing. The $P6/P7$ centers were first observed by electron paramagnetic resonance (EPR) in heat-treated n-type 6H-SiC [4] and were later shown to be a common defect in as-grown n-type [5] and high-purity semi-insulating (HPSI) [6,7] SiC. Based on their symmetry (axial or C_{3v} for $P6$ and monoclinic or C_{1h} for $P7$), $P6/P7$ centers were suggested to be the divacancy [4]. In a study using magnetic circular dichroism of the absorption (MCDA), MCDA-detected EPR, and *ab initio* calculations [8], $P6/P7$ centers were instead assigned to the photoexcited triplet state of the carbon vacancy-carbon antisite pair in the doubly positively charged state $V_C C_{Si}^{2+}$. The formation of the center was suggested to be due to the migration of a nearest C neighbor into the silicon vacancy (V_{Si}) [8]. The process $V_{Si} \rightarrow V_C C_{Si}$ is theoretically predicted to have a low reaction barrier ($\sim$1.7 [8] and $\sim$2.5 eV [2]) and can therefore be a dominating process. For SiC, so far there is no experimental evidence that the reaction $V_{Si} + V_C \rightarrow V_C V_{Si}$ is important and that the divacancy is a common defect. In a previous EPR study of HPSI SiC substrates [7], a very stable center SI-5 was assigned to the divacancy. However, in a recent EPR study [9], a symmetry lowering of SI-5 from C_{3v} to C_{1h} and additional large hyperfine (hf) interactions with ^{29}Si were observed that invalidated this model. Indeed, recent EPR studies [9] and supercell calculations [10] identify SI-5 as the carbon vacancy-carbon antisite pair in the negative charge state $V_C C_{Si}^{-}$.

In this Letter, we present results from EPR studies and *ab initio* supercell calculations which confirm that $P6/P7$ are originating from the triplet ground states of the neutral divacancy in the C_{3v}/C_{1h} configurations.

Samples used in the study are N-doped n-type (concentration $\sim 1 \times 10^{17}$ cm^{-3}), Al-doped p-type ($\sim 1 \times 10^{18}$ cm^{-3}), and HPSI 4H-SiC. In HPSI samples, the concentration of N is $\sim 1 - 5 \times 10^{15}$ cm^{-3}. The irradiation by 3 MeV electrons was performed at room temperature with a dose of 2×10^{18} cm^{-2}. For some n-type samples, the irradiation was performed at 850 °C with doses of 2×10^{18} cm^{-2} and 1×10^{19} cm^{-2}. EPR measurements were performed on Bruker ER200D and E580 X-band spectrometers. For light illumination, a Xenon lamp (150 W) was used in combination with a Jobin-Yvon 0.25 m grating monochromator and/or different optical filters.

The $P6/P7$ spectra can be detected after irradiation but are weak. The signals reach the maximum after annealing at $\sim$850 °C. In irradiated p-type 4H-SiC, the spectra can be detected only under illumination with light of photon energies $\geq$ 1.1 eV. However, in heavily irradiated (1×10^{19} cm^{-2}) n-type samples, the spectra can be detected in darkness in the whole temperature range of 4–293 K. Figure 1 shows the $P6/P7$ spectra measured in darkness at 8 K. We labeled the $P6$ spectra according to Ref. [11] and the corresponding C_{1h} spectra as $P7b$ and $P7'b$. The g value for $P6/P7$ is 2.003; the axially symmetric D and anisotropic E values of the fine structure parameter

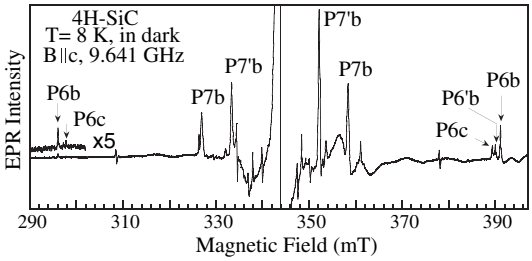

FIG. 1. EPR spectrum of $P6/P7$ centers measured for $\boldsymbol{B} \parallel \mathbf{c}$ in irradiated and annealed (850 °C) n-type 4H-SiC at 8 K in dark.

(in units of 10^{-4} cm^{-1}) are determined as: $D(P6b) = D(P7b) = 447$, $D(P6'b) = 436$, $D(P7'b) = 408$, $E(P7b) = 90$, and $E(P7'b) = 10$. The angle between the principal axis of the fine structure tensor and the c axis for $P7b$ and $P7'b$ is 70.5° and 71°, respectively.

Detailed hf structures of the low-field lines of $P6b$ and $P6'b$ spectra measured for the magnetic field $\boldsymbol{B} \parallel \boldsymbol{c}$ are shown in Fig. 2(a). Similar structures are also detected for the high-field lines. The intensity ratio between two outer hf lines and the central lines is ~3.3%–3.4%, which is approximately the natural abundance of three ^{13}C nuclei ($I = 1/2$, 1.1%). These outer hf lines are therefore assigned to the hf interaction with three nearest C neighbors (labeled C_I). The two inner hf structures can be well resolved for $P6'b$ [Fig. 2(a)]. Within the experimental error, the inner hf structures are isotropic and their intensity ratios agree well with the interaction with three and six ^{29}Si nuclei ($I = 1/2$, 4.7%). For $P7b$ and $P7'b$, similar hf interactions with three ^{13}C nuclei can also be detected at some angles. Figure 2(b) shows the hf structures of $P7b$ and $P7'b$ measured at direction of ~70° off the c axis.

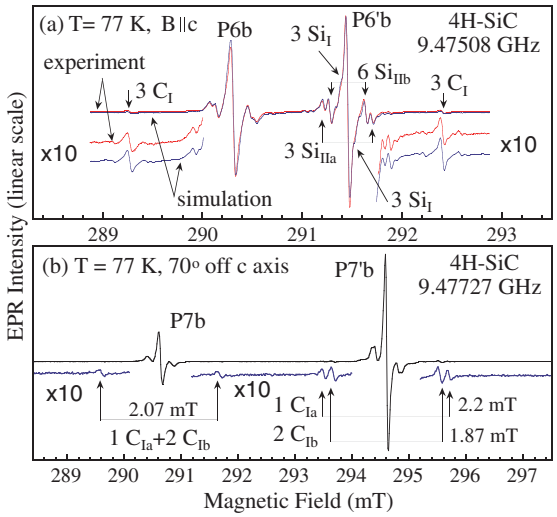

FIG. 2 (color online). EPR spectra of $P6/P7$ centers observed in irradiated and annealed (850 °C) HPSI 4H-SiC at 77 K under illumination (photon energies ~1.1–1.7 eV), showing hf structures of (a) $P6b/P6'b$ lines at $\boldsymbol{B} \parallel \mathbf{c}$ and (b) $P7b/P7'b$ lines at ~70° from the c axis.

The axial (C_{3v}) and monoclinic (C_{1h}) configurations of the divacancy are illustrated in Figs. 3(a) and 3(b), respectively. For $P6b$ and $P6'b$, the best fits to the inner hf structures are obtained with the hf tensors of 3 Si atoms on the bonds along the c axis, labeled Si$_{IIa}$, and 6 Si atoms in the plane, labeled Si$_{IIb}$ [see Fig. 3(a)]. The simulation of the $P6b$ and $P6'b$ lines and their hf structures are plotted in Fig. 2(a). The simulation includes the following hf interactions with: (i) 3 C_I nearest neighbors of V_{Si}, (ii) 3 Si$_{IIa}$ and 6 Si$_{IIb}$ second neighbors of V_{Si}, and (iii) 3 nearest Si$_I$ neighbors of V_C. As can be seen in ×10 scale spectra in Fig. 2(a), the simulation describes perfectly the observed spectra, not only the intensity of the hf lines but also their detailed superhyperfine structures.

The angular dependences of the C_I hf splitting of $P6b$ and $P6'b$ with $\boldsymbol{B}$ rotating in the $(11\bar{2}0)$ plane are shown in Fig. 3(c). These hf tensors have C_{1h} symmetry and their principal values obtained from the fit are given in Table I. The hf interactions with the nearest C_{Ia} and C_{Ib} neighbors of $P7'b$ were also observed for some crystal directions as shown in Fig. 3(d). The C_{Ib} hf tensor has C_{1h} symmetry and is similar to that observed for the nearest C_I neighbors of $P6b/P6'b$. The principal values of the C_I, C_{Ia}, and C_{Ib} hf tensors are given in Table I. The hf structures of $P7b$ detected at some directions between 60°–90° show to be similar to that of $P7'b$ [Fig. 2(b)]. The broad inner hf lines of $P7b$ and $P7'b$ are unresolved, corresponding to splitting of 0.3–0.46 mT or ~9–13 MHz. Their intensity ratios correspond to the interaction with nine Si atoms.

The observation of the $P6/P7$ spectra in dark at low temperatures confirms that these centers are related to the ground triplet state. From the above analysis of the hf

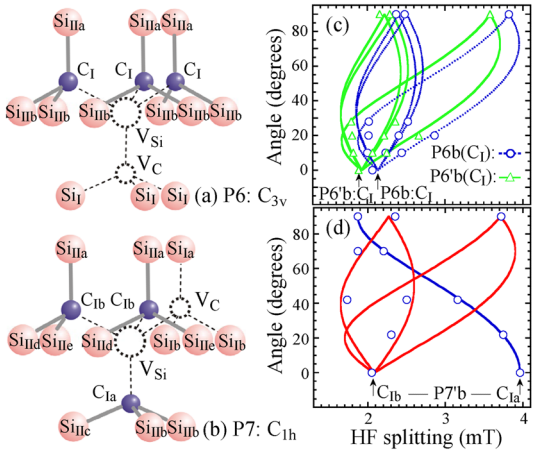

FIG. 3 (color online). Si and C neighbors of the divacancy in (a) axial (C_{3v}) and (b) monoclinic (C_{1h}) configurations. Angular dependence with $\boldsymbol{B}$ rotating in the $(11\bar{2}0)$ plane of the hf splitting of (c) C_I nearest neighbors of $P6b/P6'b$ and (d) C_{Ia} and C_{Ib} nearest neighbors of $P7'b$. For $P6b$ and $P6'b$, a misalignment of 1.5° off the $(11\bar{2}0)$ plane toward the $[\bar{1}100]$ direction was taken into account in the simulation.

TABLE I. Principal values (in MHz) of hf tensors of C and Si neighbors determined for $P6b/P6'b$ and $P7'b$ and calculated for C_{3v} and C_{1h} configurations of the neutral divacancy at cubic (k) and hexagonal (h) sites in 4H-SiC. θ is the angle between the principal z axis of the hf tensor and the c axis. The number of equivalent atoms is shown in parentheses. For C_{1h} centers, the calculated hf constants of Si_{IIa}–Si_{IIe} vary in the range ~6–10 MHz, and the obtained values for Si_{Ia} and Si_{Ib} are similar to that of C_{3v} centers. For $P7b/P7'b$, the hf interactions with 9 Si atoms were measured in the range of ~9–13 MHz.

C_{3v} center	$P6b$				$[V_{Si}(h)\text{-}V_C(h)]^0$				$P6'b$				$[V_{Si}(k)\text{-}V_C(k)]^0$			
	A_{xx}	A_{yy}	A_{zz}	θ	A_{xx}	A_{yy}	A_{zz}	θ	A_{xx}	A_{yy}	A_{zz}	θ	A_{xx}	A_{yy}	A_{zz}	θ
$C_I(\times 3)$	53	50	110	73°	55	56	116	73°	47	45	104	73°	49	49	110	73°
$Si_{IIa}(\times 3)$	12	12	12		9	9	9		13	13	13		10	10	9	
$Si_I(\times 3)$	3	3	3		3	4	5		3	3	3		1	1	2	
$Si_{IIb}(\times 6)$	9	9	9		9	9	8		10	10	10		10	10	9	
C_{1h} center	$P7b$				$[V_{Si}(h)\text{-}V_C(k)]^0$				$P7'b$				$[V_{Si}(k)\text{-}V_C(h)]^0$			
$C_{Ia}(\times 1)$	Not determined				51	52	118	2°	52	52	110	0°	52	52	116	2°
$C_{Ib}(\times 2)$	Not determined				50	50	109	70°	48	45	109	70°	43	47	103	70°

interactions, the neutral divacancy appears to be the most probable model for the $P6/P7$ centers.

We have performed *ab initio* supercell calculations of the neutral divacancy in 4H-SiC using supercells containing 256 lattice sites. For the optimization of the geometry, we employed pseudopotential methods, namely, the SIESTA code with double-ζ polarized basis set for both C and Si atoms [12] and the FHI96SPIN plane wave code with a well-converged basis set (cutoff energy of 30 Ry) [13], to check the results. The calculations were based on the local spin density approximation (LSDA: Ceperley-Alder as parametrized by Perdew and Zunger) and norm-conserving Troullier-Martins pseudopotentials [12,13]. We found that the optimized geometries of the divacancies obtained by both codes practically agreed. The hf tensors were then calculated by the all electron projector augmentation wave method using the above LSDA functional [14]. In the latter calculations, we applied a 30 Ry cutoff for the plane-waves basis set and one projector for each angular momentum in the projectors of C and Si atoms. This methodology has proven to be very successful in the study of V_C in 4H-SiC [15]. We verified that the well-known band gap failure of the LSDA did not affect our results for the ionization energies beyond the expected accuracy by applying a scissors operator to open the LSDA band gap to the experimental value as suggested by Baraff and Schlüter [16]. With this *ad hoc* correction, we assured also that the defect spin density is not tightly coupled to the energetic position of the conduction band states. We found the same hf tensors within the achievable accuracy. The obtained hf constants for different configurations are given in Table I. We found that the ground state of the neutral divacancy is a high spin state with $S = 1$. In the axial configurations, two doubly degenerate e levels appear in the band gap: The first one is below the midgap arising from C dangling bonds of V_{Si}, while the second one is above the midgap arising from Si dangling bonds of V_C. In the neutral charge state, the lower e level is occupied by two electrons with parallel spins making the defect Jahn-Teller stable. As a consequence, the spin density is mainly localized on the nearest carbon neighbors of V_{Si}, whereas the contribution of the dangling bonds at V_C is almost negligible. In the off-axis C_{1h} configurations, the situation is very similar apart from the small splitting of the degenerate e levels due to the low symmetry. The calculated $(+|0)$ and $(0|-)$ levels are at ~0.5 and ~1.4 eV above the valence band, respectively. The neutral charge state with $S = 1$ is the ground state of the divacancy when the Fermi level is in this range.

As can be seen in Table I, the principal values and the direction of the symmetry axis of the hf tensors of nearest C neighbors obtained from EPR are in good agreement with the calculated values for the neutral divacancy. Even small differences in the hf tensors of $P6b$ and $P6'b$ are also observed by EPR and calculations. Therefore, we assign $P6b$ and $P6'b$ to the axial C_{3v} configurations of the neutral divacancy at the hexagonal (h) and cubic (k) sites, respectively. Since the C_{Ia} and C_{Ib} hf tensors were not determined for $P7b$, an unambiguous identification of individual C_{1h} configurations is not possible. Using the linear combination of atomic orbital analysis, the spin density on a nearest C neighbor is determined as: ~1.8%–1.9% on the s orbital and ~18%–19% on the p orbital for $P6b$, $P6'b$, and $P7'b$. The total spin density on the three nearest C neighbors of the neutral divacancy is ~60% for the C_{3v} configuration ($P6b/P6'b$) and ~62% for the C_{1h} configuration ($P7'b$). The spin localization on three nearest Si neighbors of V_C (Si_I or Si_{Ia} and Si_{Ib}) is negligible (~ 1%).

In the previous annealing studies [11,17], the annealing characteristic of the Si vacancy (T_{V2a} center) and $P6/P7$ centers was interpreted in terms of the theoretically predicted transformation of V_{Si} into $V_C C_{Si}$. The reidentification of the $P6/P7$ centers with the divacancy demands a reinterpretation of its annealing behavior. Although a full analysis is beyond the scope of the present Letter, we briefly discuss here our annealing experiments performed for two sets of as-grown HPSI 4H-SiC samples: (i) No. 1 with strong signals of V_{Si} (T_{V2a} center), SI-5 (i.e., $V_C C_{Si}^-$ center [9,10]), and V_C^+ (EI5 center [7]); (ii) No. 2 with

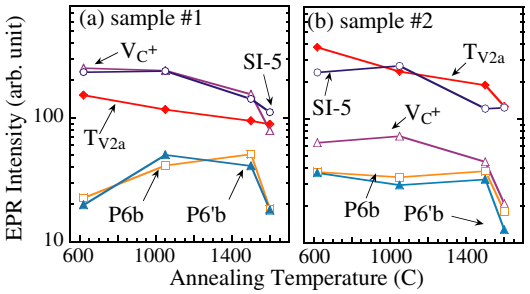

FIG. 4 (color online). Annealing temperature dependence of EPR centers in as-grown HPSI 4H-SiC samples with (a) strong signals of T_{V2a} (or V_{Si}), SI-5 (i.e., $V_C C_{Si}^-$) and V_C^+, (b) strong T_{V2a} and SI-5 and weak V_C^+ signals. The V_C^+, T_{V2a}, and $P6b/P6'b$ signals were detected under illumination (photon energies ~1.1–1.7 eV) and the SI-5 signal was detected in dark.

strong signals of V_{Si} and SI-5 and a weak V_C^+ signal. Each annealing was conducted in Ar ambient in the chemical vapor deposition reactor for 10 minutes. The natural cooling rate of the reactor after crystal growth was applied here. Since the heating/cooling time varied with temperature, the annealing is not isochronal. In both sample sets, the V_C^+, T_{V2a}, and $P6b/P6'b$ signals were detected under illumination (photon energies ~1.1–1.7 eV), whereas the SI-5 signal can be detected in dark or under illumination. The annealing temperature dependences of EPR centers in the sample sets No. 1 and No. 2 are shown in Figs. 4(a) and 4(b), respectively. Note that the EPR intensity measured under illumination depends also on the excitation efficiency and, hence, may not reflect the real defect concentration. Nevertheless, the experiment clearly shows that the annealing characteristics of $P6b/P6'b$ centers depend on the presence of other defects. Its increase in samples No. 1 [Fig. 4(a)] may be due to two processes: (i) $V_C + V_{Si} \rightarrow V_C V_{Si}$ governed by the diffusion of V_{Si} (above 700 °C) and V_C (above 1100 °C [17]), and (ii) $V_C + V_C C_{Si} \rightarrow V_C V_{Si}$ governed by the migration of V_C and $V_C C_{Si}$ (above 1100 °C). In samples No. 2, below 1500 °C the $P6$ signal is almost unchanged [Fig. 4(b)]. This suggests that both the processes (i) and (ii) are less efficient when the concentration of V_C is low. The transformation of the Si vacancy (T_{V2a}) into the antisite-vacancy pair (SI-5) is observed at temperatures about 1000 °C [Fig. 4(b)]. At higher temperatures, the dissociation of antisite-vacancy pairs seems to occur, slowing down the decrease of the V_{Si} signal [Fig. 4(b)]. This annealing behavior is in accordance with the theoretical predictions of the formation and dissociation of antisite-vacancy defects [2,8]. In both types of samples, the dissociation of the divacancy starts at ~1600 °C.

In summary, based on EPR observation and *ab initio* supercell calculations, we identified the $P6/P7$ centers in 4H-SiC to be related to the ground triplet state of the neutral divacancy in the C_{3v}/C_{1h} configurations and assigned the $P6b$ and $P6'b$ axial centers to the C_{3v} configuration at the hexagonal and cubic site, respectively. The spin density is found to be located mainly on three nearest C neighbors of V_{Si}, whereas it is negligible on the nearest Si neighbors of V_C. The vacancy model for $P6/P7$ centers also implies that the interaction between V_{Si} and V_C to form divacancies is significant and the divacancy is a common defect in SiC. Annealing studies suggest that the formation of the divacancy is governed mainly by diffusion of V_C and V_{Si}.

Support from the Swedish Foundation for Strategic Research program SiCMAT, the Swedish National Infrastructure for Computing Grant No. SNIC 011/04–8, the Swedish Foundation for International Cooperation in Research and Higher Education, the Deutsche Forschungsgemeinschaft (SiC-research group and BO 1851/2-1), and the Hungarian OTKA Grant No. F-038357 is acknowledged.

[1] L. Torpo, T. E. M. Staab, and R. M. Nieminen, Phys. Rev. B **65**, 085202 (2002).
[2] M. Bockstedte, A. Mattausch, and O. Pankratov, Phys. Rev. B **69**, 235202 (2004).
[3] U. Gerstmann, E. Rauls, and H. Overhof, Phys. Rev. B **70**, 201204(R) (2004).
[4] V. S. Vainer and V. A. Il'in, Sov. Phys. Solid State **23**, 2126 (1981).
[5] N. T. Son, Mt. Wagner, E. Sörman, W. M. Chen, B. Monemar, and E. Janzén, Semicond. Sci. Technol. **14**, 1141 (1999).
[6] W. E. Carlos, E. R. Glaser, and B. V. Shanabrook, Physica (Amsterdam) **340B–342B**, 151 (2003).
[7] N. T. Son, B. Magnusson, Z. Zolnai, A. Ellison, and E. Janzén, Mater. Sci. Forum **457–460**, 437 (2004), and references therein.
[8] Th. Lingner *et al.*, Phys. Rev. B **64**, 245212 (2001).
[9] T. Umeda, N. T. Son, J. Isoya, N. Morishita, T. Ohshima, H. Itoh, and E. Janzén, Mater. Sci. Forum (to be published).
[10] M. Bockstedte, A. Gali, T. Umeda, N. T. Son, J. Isoya, and E. Janzén, Mater. Sci. Forum (to be published).
[11] M. V. B. Pinheiro *et al.*, Phys. Rev. B **70**, 245204 (2004).
[12] A. Gali, P. Deák, P. Ordejón, N. T. Son, E. Janzén, and W. J. Choyke, Phys. Rev. B **68**, 125201 (2003).
[13] M. Bockstedte, A. Mattausch, and O. Pankratov, Phys. Rev. B **68**, 205201 (2003).
[14] P. E. Blöchl, C. J. Först, and J. Schimpl, Bull. Mater. Sci. **26**, 33 (2003).
[15] T. Umeda, J. Isoya, N. Morishita, T. Ohshima, T. Kamiya, A. Gali, P. Deák, N. T. Son, and E. Janzén, Phys. Rev. B **70**, 235212 (2004); **71**, 193202 (2005).
[16] G. A. Baraff and M. Schlüter, Phys. Rev. Lett. **55**, 1327 (1985).
[17] Z. Zolnai, N. T. Son, C. Hallin, and E. Janzén, Mater. Sci. Forum **457–460**, 473 (2004); J. Appl. Phys. **96**, 2406 (2004).